Wide-Band Multiport Antenna Characterization by Polarimetric RCS Measurements

Werner Wiesbeck, *Fellow, IEEE,* and Eberhardt Heidrich, *Senior Member, IEEE*

***Abstract*— A theoretical description of the scattering of multiport antennas is derived in accordance with the polarimetric radar target characterization. For two-port antennas with dual linear orthogonal polarization, a procedure for the determination of the antenna mode scattering parameters and the structural scattering parameters of the complete polarimetric antenna scattering matrix $[\underline{S}]$ is given. A measurement setup and experimental results of wide-band polarimetric radar cross section (RCS) antenna measurements are presented. For two-port antennas, in total, 24 unknowns have to be determined. The load variation method is used. The polarimetric RCS antenna measurement is especially advantageous over a wide bandwidth; for example 2–40 GHz with only one single calibration. From the antenna scattering matrix $[\underline{S}]$, the antenna parameters like polarimetric gain, optimum gain, gain bandwidth, wave admittance, structural scattering, etc., are derived. Results are shown for an X-band horn antenna and a 2–18-GHz dual linearly polarized horn. The measurement technique and evaluation gives the most complete and very accurate information about antenna radiation, antenna characteristics, and scattering obtainable with one single measurement setup. Some quantities determined here, like the maximum available gain and the polarization characteristics, are difficult to access with standard transmission measurements. No cable from the antenna to the receiver is necessary. This helps avoid some difficulties usually experienced at low signal levels.**

***Index Terms*—Antennas, antenna measurements, polarimetry.**

I. Introduction

SEVERAL approaches have been made to determine antenna characteristics by radar cross section (RCS) measurements and the subject has been given continuous interest since its first introduction by King in 1947 [1]. Several authors [2]–[5] have pointed out the advantages of the method compared to transmission-type measurements and slight modifications to the original sliding short-load techniques have been suggested recently by Lambert *et al.* [6]. The proposed RCS methods were restricted to the determination of the antenna gain alternatively to the conventional two-antenna, three-antenna, or gain comparison procedures. Separation of structural antenna scattering has always been the most severe problem and usually polarization properties as well as matching conditions on the antenna feed terminals were not considered properly.

The antenna scattering is characterized by the structural scattering and load mismatch reflections, as shown in Fig. 1.

Manuscript received September 30, 1996; revised September 1, 1997.

W. Wiesbeck is with the Institut für Höchstfrequenztechnik und Elektronik, University Karlsruhe, Karlsruhe, 76128 Germany.

E. Heidrich is with L&S Höchfrequenztechnik GmbH, Lichtenau, 77839 Germany.

Publisher Item Identifier S 0018-926X(98)02255-8.

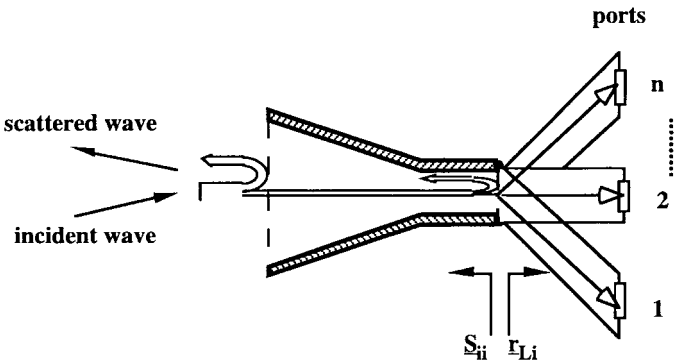

Fig. 1. Incident wave, structural scattering, and reradiation from load reflection of a multiport antenna.

Both are frequency and polarization dependent and both interact with each other. As these processes involve all antenna characteristics that are of interest, it should be possible to determine them from RCS measurements.

An approach has been presented in [7] and [8] in which the single-port antenna is treated as a loaded polarimetric scatterer. The typical characteristics of an antenna as a radar target have been dealt with in [9]. All interactions of incident, scattered, absorbed, and reradiated waves are incorporated in a polarization-dependent network model. The model parameters can be related to the conventionally used antenna characteristics [10] like gain, polarization, axial ratio, and polarization decoupling. It has also been shown that both input impedance and structural scattering can be obtained with one single measurement setup.

This paper extends the network description and measurement procedure to multiport antennas. In practice, antennas with one or two excitation ports (e.g., two polarizations or dual-frequency operation) are of special interest. The multiport theory is applied to these antennas. Measurement results are presented for waveguide and planar antennas. Advantages and limitations of the method are discussed.

II. Polarimetric Antenna RCS Matrix and Multiport Antenna Model

A. Derivation of the General Antenna Scattering Matrix

For fixed frequency and aspect angle, any radar target's scattering behavior is completely defined by the complex polarimetric RCS matrix $[\underline{\sigma}]$ or Sinclair matrix $[\underline{S}]$ for dual

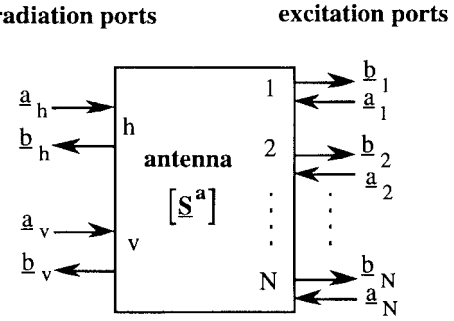

Fig. 2. Antenna as a $N+2$-port network: two dual-orthogonal radiation ports; N excitation ports.

orthogonal polarizations ξ and η as given in

$$[\underline{\sigma}] = \begin{bmatrix} \underline{\sigma}_{\xi\xi} & \underline{\sigma}_{\xi\eta} \\ \underline{\sigma}_{\eta\xi} & \underline{\sigma}_{\eta\eta} \end{bmatrix} = \begin{bmatrix} \underline{S}^2_{\xi\xi} & \underline{S}^2_{\xi\eta} \\ \underline{S}^2_{\eta\xi} & \underline{S}^2_{\eta\eta} \end{bmatrix}. \tag{1}$$

In (1), the $\underline{S}_{ij}$ are the range-independent object-related scattering coefficients [11]. This definition implies that $\underline{S}_{\xi\eta} = \sqrt{\underline{\sigma}_{\xi\eta}/m^2}$, with m^2 being square meters. Detailed information on polarimetry and antenna polarization aspects is given by Mott *et al*. in [10] and [12].

An antenna can be treated as a generalized scattering object with one or more excitation ports connected. A convenient way for the description of the interaction between internal and external antenna fields and waves is by power waves and scattering parameters, known from network theory. For that purpose, different ports have to be defined for the antenna (Fig. 2). The port definition is easily applied to the N excitation ports of the antenna where transmission lines with well definable reference planes exist. The radiation from the antenna is decomposed into two ports for orthogonal polarizations (e.g., horizontal and vertical as used in the following) according to the matrices $[\underline{\sigma}]$ or $[\underline{\boldsymbol{S}}]$ in (1). The use of dual-linear orthogonal polarizations is no restriction, as any other polarization basis can be chosen by linear basis transformation [12]. This multiport description contains all interactions between the incident, scattered, reradiated, and absorbed fields of the antenna.

For an antenna with N excitation ports, an $(N+2)$ antenna scattering matrix results [according to (2)] with the incident power wave vector $[\underline{\boldsymbol{a}}]$ and the output power wave vector $[\underline{\boldsymbol{b}}]$

$$\begin{bmatrix} \underline{b}_h \\ \underline{b}_v \\ \underline{b}_1 \\ \cdot \\ \underline{b}_N \end{bmatrix} = \left[\begin{array}{cc|ccc} \underline{S}^s_{hh} & \underline{S}^s_{hv} & \underline{S}_{h1} & \cdot & \underline{S}_{hN} \\ \underline{S}^s_{vh} & \underline{S}^s_{vv} & \underline{S}_{v1} & \cdot & \underline{S}_{vN} \\ \hline \underline{S}_{1h} & \underline{S}_{1v} & \underline{S}_{11} & \cdot & \underline{S}_{1N} \\ \cdot & \cdot & \cdot & \cdot & \cdot \\ \underline{S}_{Nh} & \underline{S}_{Nv} & \underline{S}_{N1} & \cdot & \underline{S}_{NN} \end{array}\right] \begin{bmatrix} \underline{a}_h \\ \underline{a}_v \\ \underline{a}_1 \\ \cdot \\ \underline{a}_N \end{bmatrix}$$

$$= [\underline{\boldsymbol{S}}^a] \begin{bmatrix} \underline{a}_h \\ \underline{a}_v \\ \underline{a}_1 \\ \cdot \\ \underline{a}_N \end{bmatrix}. \tag{2}$$

The antenna scattering matrix $[\underline{\boldsymbol{S}}^a]$ can be divided into four submatrices as indicated by the dashed lines in (2). Submatrix [1] describes the *structural antenna scattering*, with the excitation ports terminated in matched loads $(\underline{a}_1, \underline{a}_2, \cdots \underline{a}_N = 0)$. The submatrices [2] and [3] connect excitation ports with radiation ports and describe the *transmit and receive characteristics* of the antenna. Submatrix [4] contains only parameters of the excitation ports with the *input reflection coefficients* in the main diagonal and the coupling between the antenna feed lines described by the other elements. These coupling parameters take into account all coupling effects, e.g., field coupling or feed network coupling. In (2), reciprocity is not required, i.e., $[\underline{\boldsymbol{S}}^a]$ is not necessarily to be $[\underline{\boldsymbol{S}}^a]^T$.

If the excitation ports are terminated with load impedances $\underline{Z}_{Li}$ corresponding to load reflection coefficients $\underline{r}_{Li}$

$$\underline{r}_{Li} = \frac{\underline{b}_{Li}}{\underline{a}_{Li}} = \frac{\underline{a}_i}{\underline{b}_i} = \frac{\underline{Z}_{Li} - \underline{Z}_0}{\underline{Z}_{Li} + \underline{Z}_0}; \quad \underline{Z}_0 = \text{reference plane} \tag{3}$$

only the two radiation ports h and v of the network in Fig. 2 remain. The $(N+2)$ antenna scattering matrix $[\underline{\boldsymbol{S}}^a]$ reduces to the two-port object-related *total scattering matrix* $[\underline{\boldsymbol{S}}^{\mathrm{tot}}]$ as follows:

$$\begin{bmatrix} \underline{b}_h \\ \underline{b}_v \end{bmatrix} = [\underline{\boldsymbol{S}}^{\mathrm{tot}}] \begin{bmatrix} \underline{a}_h \\ \underline{a}_v \end{bmatrix}$$

$$= \left[\underbrace{\begin{bmatrix} \underline{S}^{\mathrm{tr}}_{hh} & \underline{S}^{\mathrm{tr}}_{hv} \\ \underline{S}^{\mathrm{tr}}_{vh} & \underline{S}^{\mathrm{tr}}_{vv} \end{bmatrix}}_{[\underline{\boldsymbol{S}}^{\mathrm{tr}}]} + \underbrace{\begin{bmatrix} \underline{S}^{s}_{hh} & \underline{S}^{s}_{hv} \\ \underline{S}^{s}_{vh} & \underline{S}^{s}_{vv} \end{bmatrix}}_{[\underline{\boldsymbol{S}}^{s}]} \right] \begin{bmatrix} \underline{a}_h \\ \underline{a}_v \end{bmatrix}. \tag{4}$$

In (4), the total scattering matrix $[\underline{\boldsymbol{S}}^{\mathrm{tot}}]$ is the sum of two square matrices, the *transfer matrix* $[\underline{\boldsymbol{S}}^{\mathrm{tr}}]$, and the *structural scattering matrix* $[\underline{\boldsymbol{S}}^s]$. The transfer matrix $[\underline{\boldsymbol{S}}^{\mathrm{tr}}]$ contains the products of transmit, receive, and excitation port parameters and there is no simple, general mathematical representation. However, if all coupling terms between the waveguide ports are neglected ($S_{ij} = 0$ for all $i \neq j$), only the elements in the main diagonal remain in submatrix [4]. For this case, the transfer matrix is given as a sum of N single transfer matrices as

$$[\underline{S}^{\mathrm{tr}}] = \sum_{i=1}^{N} [\underline{\boldsymbol{S}}^{\mathrm{tr}}]_{(i)}, \qquad \text{for } \underline{S}_{ij} = 0, i \neq j \tag{5}$$

with

$$[\underline{\boldsymbol{S}}^{\mathrm{tr}}]_{(i)} = \frac{\underline{r}_{Li}}{1 - \underline{S}_{ii}\underline{r}_{Li}} \begin{bmatrix} \underline{S}_{hi}\underline{S}_{ih} & \underline{S}_{hi}\underline{S}_{iv} \\ \underline{S}_{vi}\underline{S}_{ih} & \underline{S}_{vi}\underline{S}_{iv} \end{bmatrix} \tag{6}$$

which means that the antenna consists of N single antennas which do not influence each other's transmit or receive characteristics.

If all waveguide ports are terminated with matched loads ($\underline{r}_{Li} = 0$ for $i = 1 \cdots N$); only the *structural scattering matrix* $[\underline{\boldsymbol{S}}^s]$ remains. This matrix contains the scattering coefficients from submatrix [1] of (2) which describe the total structural scattering of all antenna subsystems. The structural scattering is dealt with in more detail in [9].

The N-port antenna network model above applies to antenna arrays, if each antenna element out of N is regarded as a

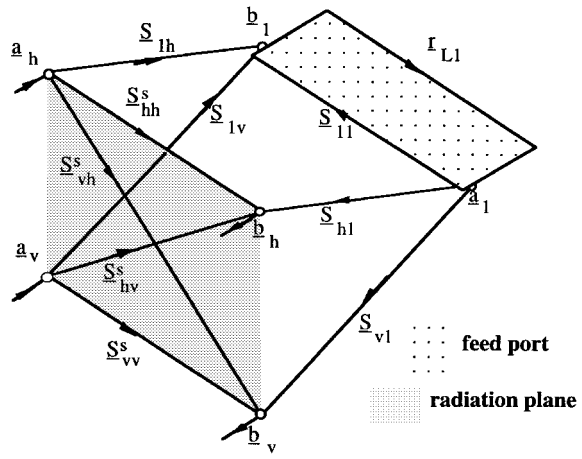

Fig. 3. Signal flow graph for a single-port antenna.

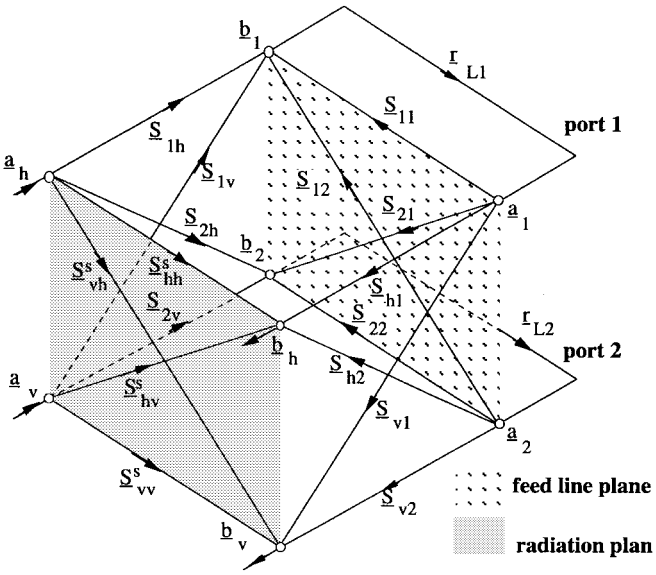

Fig. 4. Signal flow graph for a dual-port antenna.

port. In most practical cases antennas have only one (single polarization) or two (e.g., dual-orthogonal polarization) excitation ports. The scattering matrices of these antennas will be examined in more detail in the following.

B. Antennas with One and Two Excitation Ports

For antennas with one excitation port (2) reduces to a three-port-matrix with nine complex unknowns. If the excitation port is terminated with the load reflection coefficient $\underline{r}_{L1}$ a reduced total scattering matrix $[\underline{\boldsymbol{S}}^{\mathrm{tot}}]$ in (7) remains. From the transfer matrix, a common product term can be separated that contains only feed-line and load characteristics

$$[\underline{\boldsymbol{S}}^{\mathrm{tot}}] = \left[\underbrace{\frac{\underline{r}_{L1}}{1-\underline{S}_{11}\underline{r}_{L1}} \begin{bmatrix} \underline{S}_{h1}\underline{S}_{1h} & \underline{S}_{h1}\underline{S}_{1v} \\ \underline{S}_{v1}\underline{S}_{1h} & \underline{S}_{v1}\underline{S}_{1v} \end{bmatrix}}_{[\underline{\boldsymbol{S}}^{\mathrm{tr}}]} + \underbrace{\begin{bmatrix} \underline{S}^s_{hh} & \underline{S}^s_{hv} \\ \underline{S}^s_{vh} & \underline{S}^s_{vv} \end{bmatrix}}_{[\underline{\boldsymbol{S}}^s]} \right]. \tag{7}$$

The mathematical relation given in (7) can be visualized in a three-dimensional signal flow chart, as shown in Fig. 3. As the structure of such a graph is based on physical signal paths, it clearly describes the interaction of the antenna with an incident field. For example, if a horizontally polarized field with wave amplitude $\underline{a}_h$ is incident on the antenna, part of the energy will be scattered due to the antenna structure. This scattered field can be decomposed into two orthogonal components described by the signal paths $\underline{S}^s_{hh}$ (horizontal) and $\underline{S}^s_{vh}$ (diagonal). The antenna accepts energy along the path $\underline{S}_{1h}$. Depending on the load reflection coefficient $\underline{r}_{L1}$ and the antenna input reflection coefficient $\underline{S}_{11}$, the received energy will be partly absorbed in the load and partly reradiated. Since any physical antenna possesses only finite polarization purity, the reradiation occurs not only in copolarization via $\underline{S}_{h1}$, but also in cross polarization via $\underline{S}_{v1}$. The totally scattered antenna field is a superposition of structural scattering and antenna reradiation.

For an antenna with two excitation ports, (2) reduces to a four-port matrix with 16 complex unknowns. After loading the two excitation ports with $\underline{r}_{L1}$ and $\underline{r}_{L2}$, respectively, a matrix $[\underline{\boldsymbol{S}}^{\mathrm{tot}}]$ according to (4) remains. Due to of the coupling between the two excitation ports the components of $[\underline{\boldsymbol{S}}^{\mathrm{tr}}]$ have the form given in (8)

$$\begin{aligned} \underline{S}^{\mathrm{tr}}_{\xi\eta} = \frac{1}{\underline{N}} \{ & \underline{S}_{1\xi}\underline{S}_{\eta 1}\underline{r}_{L1}(1-\underline{S}_{22}\underline{r}_{L2}) + \underline{S}_{2\xi}\underline{S}_{\eta 2} \\ & \cdot \underline{r}_{L2}(1-\underline{S}_{11}\underline{r}_{L1}) + (\underline{S}_{1\xi}\underline{S}_{21}\underline{S}_{\eta 2} + \underline{S}_{2\xi}\underline{S}_{12}\underline{S}_{\eta 1}) \\ & \cdot \underline{r}_{L1}\underline{r}_{L2}\} \end{aligned} \tag{8}$$

with

$$\underline{N} = (1-\underline{S}_{11}\underline{r}_{L1})(1-\underline{S}_{22}\underline{r}_{L2}) - \underline{S}_{12}\underline{S}_{21}\underline{S}_{\eta 1})\underline{r}_{L1}\underline{r}_{L2}\}. \tag{9}$$

ξ, η polarization indexes representing the orthogonal polarizations h, v indexes 1, 2 representing excitation ports 1.

If the coupling terms $\underline{S}_{12}$ and $\underline{S}_{21}$ between the two waveguides can be neglected compared to the reflection coefficients in (9), the separation into two separate antenna subsystems [as shown in (5)] is possible.

For the antenna with two excitation ports the signal flow graph has to be expanded, as shown in Fig. 4. The signal flow graph in comparison to the one given in Fig. 3 is extended by a feed-line plane.

III. Derivation of Characteristic Antenna Parameters from the Antenna Scattering Matrix

The antenna scattering matrix $[\underline{\boldsymbol{S}}^a]$ incorporates in its submatrix $[\underline{\boldsymbol{S}}^{\mathrm{tr}}]$ the transmit/receive behavior of an antenna. This allows the derivation of the characteristic antenna quantities like gain, radiation pattern, polarization, or input impedance. In this section, the corresponding relationships are shown.

A. Antenna Polarization

For the determination of the antenna polarization, the antenna will be examined in the transmit mode ($\underline{a}_h, \underline{a}_v = 0$). The excitation port n is fed with a power wave $\underline{a}_n$ and all other excitation ports are terminated ($\underline{a}_i = 0, i = 1 \cdots N, i \neq n$). The antenna radiates an electromagnetic wave with power waves $\underline{b}_h$ and $\underline{b}_v$ according to

$$\underline{b}_h = \underline{S}_{hn}\,\underline{a}_n \tag{10a}$$

$$\underline{b}_v = \underline{S}_{vn}\,\underline{a}_n\,. \tag{10b}$$

The ratio of both power waves in (10) results in the complex polarization ratio $\underline{P}_n$

$$\underline{P}_n = \frac{\underline{b}_v}{\underline{b}_h} = \frac{\underline{S}_{vn}}{\underline{S}_{hn}} = \tan\gamma_n\, e^{j\,\delta_n} \quad \text{(excitation at port } n\text{)}. \tag{11}$$

This polarization state $\underline{P}_n$ is defined as the copolarization. Any other polarization state can be calculated from $\underline{P}_n$ by basis transformation. Alternatively, the polarization state of an electromagnetic wave can be described by the ellipticity angle α_n and the tilt angle ψ_n of the polarization ellipse. Both can be calculated from γ_n and δ_n [12], [13]. The orientation angle ψ describes the rotation of the main axis of the polarization ellipse in a plane normal to the propagation direction and the ellipticity angle α describes the axial ratio of the orthogonal polarization vectors. Waves without ellipticity ($\alpha = 0$) are linearly polarized; waves with $\alpha = \pm 45°$ are left- or right-hand circularly polarized, respectively.

For the determination of further characteristic antenna parameters for port n, the antenna transfer-matrix $[\underline{\boldsymbol{S}}^{\mathrm{tr}}]$ is transformed into a polarization basis matched to the copolarization α_n, ψ_n, as defined above. This antenna copolarization α_n, ψ_n is described by the polarization index ξ in the new basis and the cross polarization by the index η. The transformed matrix $[\underline{\boldsymbol{S}}^{\mathrm{tr}}]'$ has the following form:

$$[\underline{S}^{\mathrm{tr}}]' = \begin{bmatrix} \underline{S}^{\mathrm{tr}}_{\xi\xi} & \underline{S}^{\mathrm{tr}}_{\xi\eta} \\ \underline{S}^{\mathrm{tr}}_{\eta\xi} & \underline{S}^{\mathrm{tr}}_{\eta\eta} \end{bmatrix}. \tag{12}$$

B. Copolarization and Cross-Polarization Antenna Gain

The antenna gain G is inherent in the antenna transfer parameters. For the derivation of G from the scattering matrix description the basic relation between the RCS $\underline{\sigma}$ and G is evaluated, as it was similarly used by Appel–Hansen [3] for a short-circuited antenna ($\underline{r}_L = -1$) and for copolarization only

$$\sigma = G A_W\,. \tag{13}$$

A_W is the effective antenna area. This simple equation (13) does not regard the polarization and load mismatch. It can be extended to (14) to account for an incident wave with arbitrary polarization n and the effective antenna area $A_{Wn\mu}$ for the port n

$$|\underline{\sigma}^{\mathrm{tr}}_{\nu\mu}| = \sigma^{\mathrm{tr}}_{\nu\mu} = G_{\nu n} A_{Wn\mu} |\underline{r}_{Ln}|^2. \tag{14}$$

The energy received and reflected according to $\underline{r}_{Ln}$ is reradiated with the gain $G_{\nu n}$ of the antenna in ν polarization. $\sigma^{\mathrm{tr}}_{\nu\mu}$ can also be derived from (1), (6), and (12)

$$\sigma^{\mathrm{tr}}_{\nu\mu} = |\underline{S}^{\mathrm{tr}}_{\nu\mu}|^2 m^2 = \frac{|\underline{r}_{Ln}|^2}{|1 - \underline{S}_{nn}\underline{r}_{Ln}|^2} |\underline{S}_{\nu n}\underline{S}_{n\mu}|^2 m^2. \tag{15}$$

Note that this derivation is for port n while all other ports are terminated with matched loads. Assuming antenna reciprocity, the effective area $A_{Wn\mu}$ can be substituted with the gain $G_{\nu n}$ and also the receive transfer parameter $\underline{S}_{n\mu}$ with the transmit parameter $\underline{S}_{\nu n}$. Additionally, if the same polarization is considered for transmit and receive channels ($\nu = \mu = \zeta$) the final result for the antenna gain is

$$G_{\zeta n} = \frac{\sqrt{4\pi}}{\lambda/m} \frac{|\underline{S}_{\zeta n}|^2}{|1 - \underline{S}_{nn}\underline{r}_{Ln}|} \tag{16}$$

with $\underline{r}_{Li} = 0$ for $i \neq n, i = 1 \cdots N$.

With (16) the antenna gain can be determined for arbitrary polarizations and load impedances. A more detailed description of these relationships is given in [16].

Two gain definitions of special interest are introduced in the following. These definitions are chosen similar to the gain expressions used for active two-port networks. The first gain definition describes the *maximum available antenna* gain G^m at the antenna port n for a conjugate matched load ($\underline{r}_{Ln} = \underline{S}^*_{nn}$)

$$G^m_{n\mathrm{Co}} = \frac{\sqrt{4\pi}}{\lambda/m} \frac{|\underline{S}_{\xi n}|^2}{1 - |\underline{S}_{nn}|^2} \tag{17a}$$

$$G^m_{n\mathrm{Cross}} = \frac{\sqrt{4\pi}}{\lambda/m} \frac{|\underline{S}_{\eta n}|^2}{1 - |\underline{S}_{nn}|^2}. \tag{17b}$$

These definitions correspond to the IEEE antenna standards definition of power gain [14] and are similar to those derived by Newell *et al.* [15]. The second gain definition describes for the *transducer antenna gain* G^t, which results for antenna port n terminated in a nominal matched load ($\underline{r}_{Ln} = 0$)

$$G^t_{n\mathrm{Co}} = \frac{\sqrt{4\pi}}{\lambda/m} |\underline{S}_{\xi n}|^2 \tag{18a}$$

$$G^t_{n\mathrm{Cross}} = \frac{\sqrt{4\pi}}{\lambda/m} |\underline{S}_{\eta n}|^2. \tag{18b}$$

Examples are given in Section V-A to demonstrate the difference between these two gain definitions. The ratio of the copolarized and cross-polarized gain in (17) or (18) leads to the *polarization decoupling* of the antenna. The measurement of the maximum available gain in copolarization $G^m_{n\mathrm{Co}}$ and also the maximum available gain in cross-polarization $G^m_{n\mathrm{Cross}}$ are inherently determined over a wide bandwidth with this method.

C. Input Reflection Coefficients, Port Coupling, and Radiation Pattern

As already mentioned in Section II, submatrix [4] contains the parameters of the excitation ports where the elements $\underline{S}_{ii}$ of the main diagonal are the *input reflection coefficients* and the elements $\underline{S}_{ij}$ describe the *coupling* between the ports i and j.

If the antenna scattering matrix is determined as a function of azimuth and/or elevation, all deducible parameters (gain,

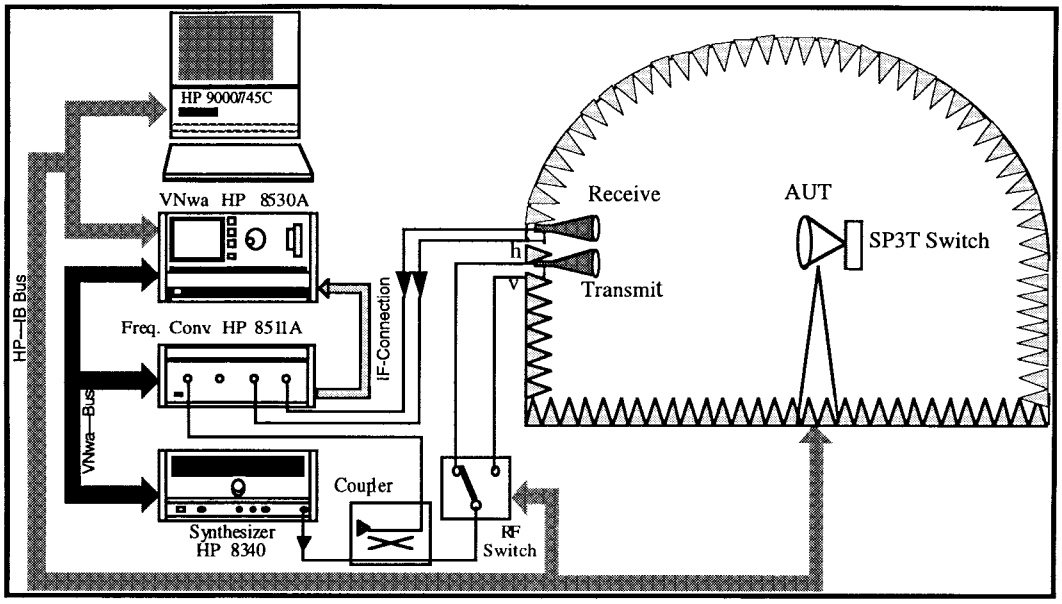

Fig. 5. Wide-band polarimetric RCS instrumentation radar system.

polarization, structural scattering) can be evaluated as a function of these angles. The *radiation pattern* of the antenna can be calculated directly from the transfer parameters in (2) and it can also be formulated in terms of antenna gain

$$C(\vartheta,\varphi)=\sqrt{\frac{G(\vartheta,\varphi)}{G(\vartheta,\varphi)_{\max}}} \tag{19}$$

$G(\vartheta,\varphi)$ = gain from (17) or (18).

Up until now, the theoretical formulations of antenna RCS characteristics are derived. Most of the necessary scattering parameters are only available from full polarimetric RCS measurement systems such as the one introduced in the following.

IV. Polarimetric RCS Antenna Measurement

A. Measurement Setup and Procedure

The measurement of the total scattering matrix $[\underline{S}^{\mathrm{tot}}]$ is performed with a wide-band polarimetric instrumentation radar system (see Fig. 5) based on a computer-controlled vector network analyzer (VNwA), as given in [11, Fig. 5]. Together with a highly sophisticated error correction and calibration procedure the system is able to measure the polarization-dependent absolute calibrated scattering matrix of an object in amplitude and phase. As it is a stepped frequency system, range reflection from areas off the antenna under test (AUT) can be eliminated by range gating. Reflections from the antenna positioner are regarded in the calibration. Interactions between the AUT and the positioner contribute to the measurement error. For high isolation between transmit and receive channels, a quasi-monostatic antenna configuration is used. The gain of an antenna in copolarization and cross-polarization is obtained in dBi without any further reference antenna because the measurement system is absolutely calibrated in decibel square meter (dBsm). The only reference is a copolarization calibration target, usually an extremely precisely manufactured metallic sphere [11].

With an RCS measurement of the loaded antenna the total antenna scattering matrix $[\underline{S}^{\mathrm{tot}}]$ in (4) is determined. For the separation of the nine (antenna with one output port) or 16 (antenna with two output ports) matrix coefficients at least an equal number of linearly independent measurements is necessary. These linearly independent measurements are achieved with the load variation principle [16]. For one excitation port, three loads are necessary; for two excitation ports, it can be shown that an advantageous procedure uses seven measurements of the matrix $[\underline{S}^{\mathrm{tot}}]$ with different load reflection coefficients $\underline{r}_{L1}$, $\underline{r}_{L2}$ to solve (4) for the single matrix coefficients. Each load (one-port antenna) or load combination (two-port antenna), respectively, results in the determination of a 2×2 scattering matrix with a total of four matrix coefficients.

For passive, linear, and isotropic antennas, the following reciprocity assumptions are made (see Mott [10]):

1) structural scattering $\underline{S}^s_{hv} = \underline{S}^s_{vh}$;
2) transfer products $\underline{S}_{ih} = \underline{S}_{hi}, \underline{S}_{iv} = \underline{S}_{vi}$;
3) feed-line coupling product $\underline{S}_{12h} = \underline{S}_{21}$.

The subscript i holds for the different excitation ports $(i = 1, 2)$. This reduces the number of 16 complex unknowns in (2) to seven complex parameters.

The load variation for the AUT is realized with remotely controlled SP3T coaxial switches for each antenna port. On the output ports of each switch the three different loads are attached (e.g., open, short, and matched load), as shown in Fig. 6. The input reflection coefficients $\underline{r}_{L1}$ and $\underline{r}_{L2}$ for the switches in each switch position are measured with a vector network analyzer over the full frequency range in sufficient small frequency increments. These data sets are stored in a software lookup table and an interpolation routine is used for intermediate values if necessary. It is required that the impedances of the matched load, open, and short behave well

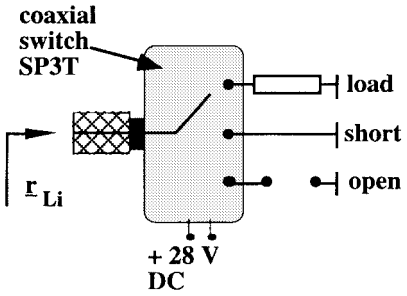

Fig. 6. Load variation circuitry with a SP3T switch.

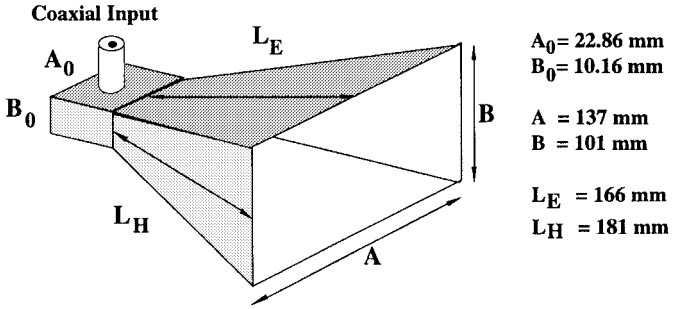

Fig. 7. X-band pyramidal horn antenna (horn 1).

and do not cross over the frequency range. Otherwise, there is no more a unique solution of the calibration process.

For the RCS measurement of a two-port antenna, the two switches are connected to the excitation ports of the AUT, the antenna is positioned on the target mount, and $[\underline{S}^{\mathrm{tot}}]$ is measured for the different switch positions and polarizations. From the nine possible load combinations $\underline{r}_{L1}, \underline{r}_{L2}$ on the two switches, only the following seven are used:

matched load — matched load
short — matched load
matched load — short
open — matched load
matched load — open
open — short
short — open.

These combinations are advantageously used for gain and polarization measurements, while combinations "open–open" and "short–short" are only preferred if there is special interest in feed-line coupling. With these combinations, it is possible to invert the matrix (4) and solve for 15 parameters or parameter products as there are:

1) structural scattering $\underline{S}_{hh}, \underline{S}_{hv}, \underline{S}_{vh}, \underline{S}_{vv}$;
2) transfer products $\underline{S}_{ih}\underline{S}_{hi}, \underline{S}_{iv}\underline{S}_{hi}, \underline{S}_{ih}\underline{S}_{vi}, \underline{S}_{iv}\underline{S}_{vi}$;
3) input-reflection coefficients $\underline{S}_{11}, \underline{S}_{22}$;
4) feed-line coupling product $\underline{S}_{12}\underline{S}_{21}$.

The subscript i holds for the different excitation ports $(i = 1, 2)$. It should be noted that for the antenna transfer characteristics as well as for the feed-line coupling only products of matrix coefficients can be determined. This is because there is no access to the internal nodes of the signal flow graph of Fig. 4. It causes no problems, as the evaluation

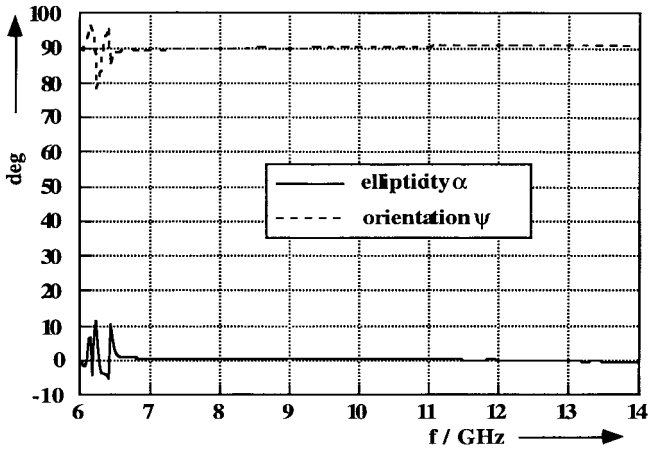

Fig. 8. Ellipticity α and orientation angle ψ of horn 1 (Fig. 7) (cutoff frequency 6.67 GHz).

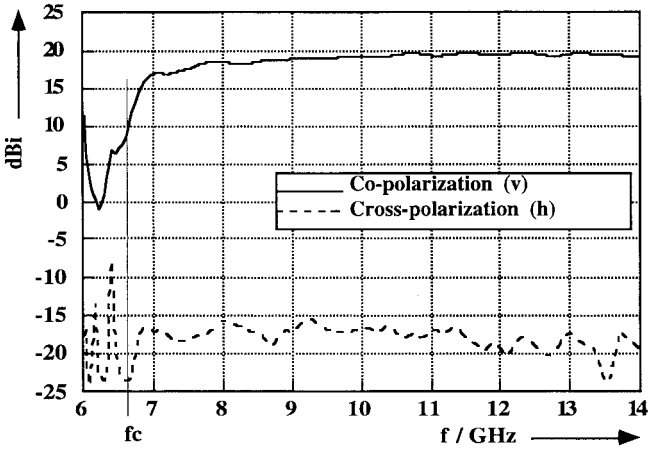

Fig. 9. Gain G^t of horn 1 (Fig. 7) in copolarization and cross polarization.

of the characteristic antenna parameters also uses only these combinations. The coefficient most difficult to measure is the feed-line coupling product $\underline{S}_{12}\underline{S}_{21}$, which will be discussed later on in more detail.

B. Measurement Uncertainties

The uncertainties of the measurements depend on the VNwA accuracy, the calibration levels, the residual systematic errors after calibration, the dynamic range, and noise. The typical error of the VNwA is 50 dB off the calibration level approximately ± 0.3 dB in amplitude and 3° in phase. At calibration level the uncertainties are less than 0.07 dB and 0.5°. The uncertainty budget for quantities determined from copolarization measurements is close to the uncertainties for calibration levels, i.e., for the copolarization gain G_{Co} is 0.08 dB. For quantities involving cross-polarization measurements, i.e., G_{Cross} the error can for a cross-polarization 40-dB below calibration level run up to 3 dB.

V. Experimental Characterization of Antennas

The efficiency and the advantages of the antenna model and measurement procedure are demonstrated in the following for wide-band horn antennas, having either one or two feed ports.

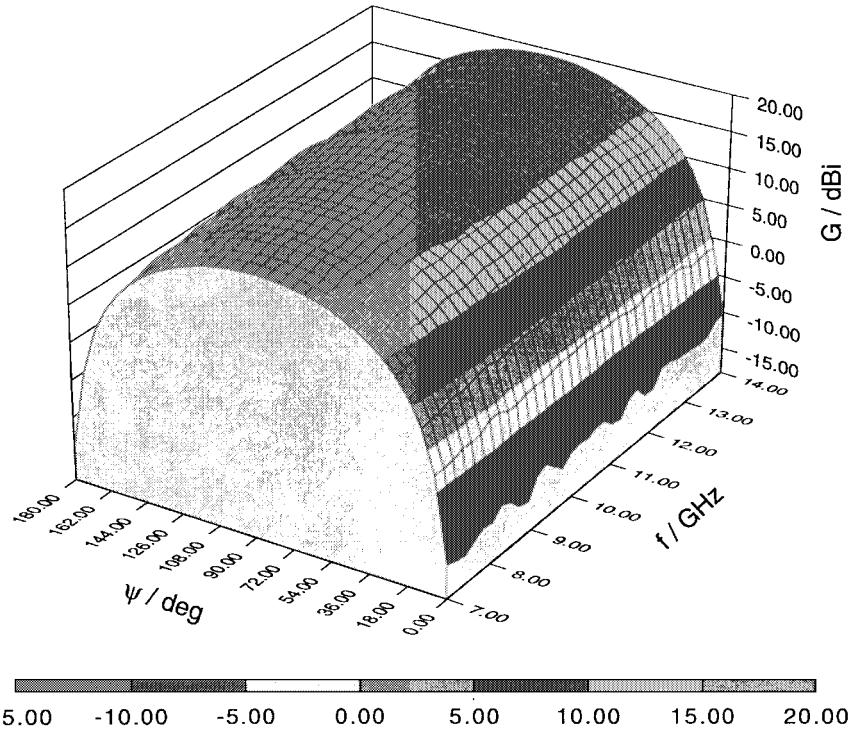

Fig. 10. Gain G^t of horn 1 (Fig. 7) versus polarization-orientation angle ψ and frequency (dispersive-polarimetric gain signature).

The range length of the measurement in the anechoic chamber is for these antennas at 10 GHz approximately $8D^2/\lambda$.

A. X-Band Pyramidal Horn Antenna

A standard X-band horn is the first test object for verification. The horn antenna is outlined in Fig. 7, the results in Figs. 8–12 and 17 are for this horn. During the measurement it is aligned for vertical copolarization. The total scattered field is measured in the frequency range from 6 to 14 GHz with 401 frequency steps. Fig. 8 shows the resulting antenna polarization parameters α and ψ versus frequency. The horn radiates an almost ideal linearly polarized wave with a very low ellipticity of $\alpha \leq 0.5°$. The orientation angle ψ is 90° and corresponds to the vertical copolarization of the horn. Fig. 9 shows the copolarized and cross-polarized gain G^t of the horn according to (18), respectively. The cutoff frequency of the X-band waveguide is 6.67 GHz. The weak undulation of the copolarized gain, usually not identified in measurements, results from the interactions of reflected waves.

For each load, the set of measurements described above, determine the complete 2 × 2 polarimetric scattering matrix of the antenna. This allows the transformation to an arbitrary polarization basis as initially stated. As a result, all the previously calculated antenna characteristics are available for arbitrary polarization [16]. This feature exceeds most other antenna measurement techniques. An example is shown in Fig. 10, where the gain G^t is plotted versus frequency and polarization. For the single port antenna the shape of the polarization dependent gain is evidently closely related to $|\sin\psi|$. The information content of this signature is much higher for circularly or arbitrary elliptically polarized antennas.

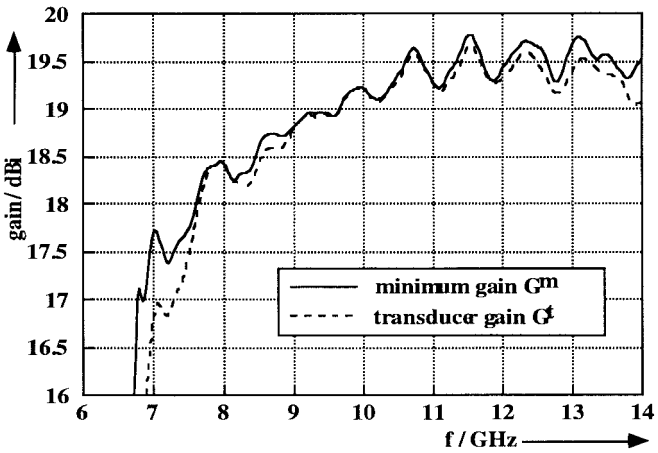

Fig. 11. Comparison of the maximum gain G^m and the transducer gain G^t of horn 1 (Fig. 7).

In Fig. 11, the two-gain definitions given in (17) (G^m_{Co}) and (18) (G^t_{Co}) are compared for the copolarization in an extended scale. Both definitions result in the same gain about the center frequency, but differ at the low and high end. This can be easily explained by the input impedance shown in Fig. 12. The antenna is well matched to its feed line near 8 GHz and also between 9 and 12 GHz with $|\underline{S}_{11}| < -20$ dB. The decreasing matching outside this frequency range results in a decrease of the antenna gain G^t. For a perfect conjugated matched load, the maximum available gain G^m can be obtained. Fig. 12 also shows the accuracy and performance of the measurement procedure and data evaluation. The solid line is $|\underline{S}_{11}|$ as derived by the far-field RCS measurement, the dashed line shows a direct measurement with a vector

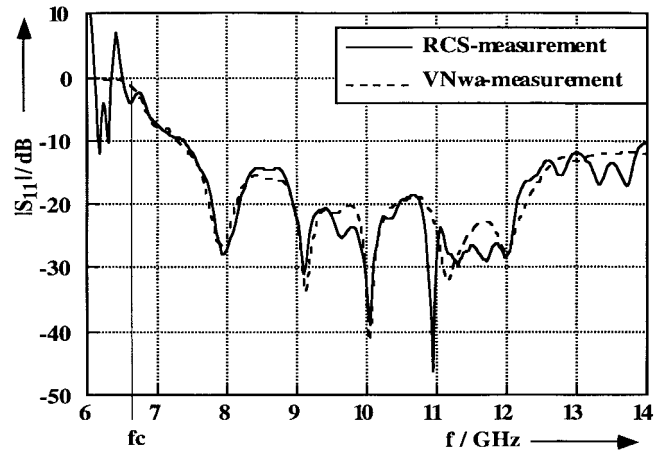

Fig. 12. Comparison of RCS and VNwa reflection-coefficient measurements of horn 1 (Fig. 7).

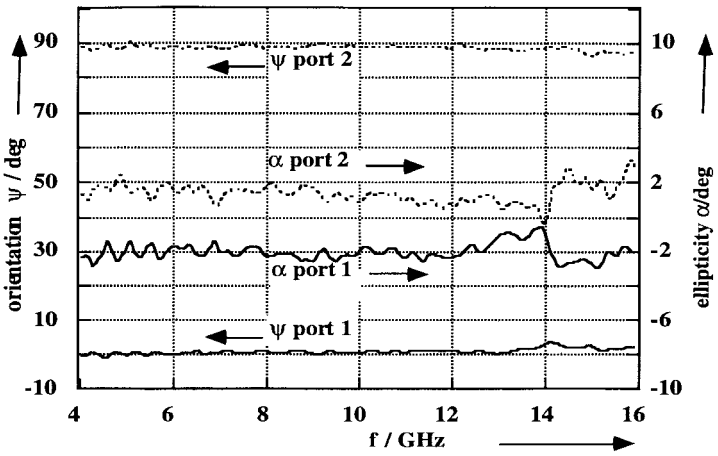

Fig. 14. Ellipticity α and rotation angle ψ of the dual-polarized broad-band horn 2 (from Fig. 13) for ports 1 and 2, respectively.

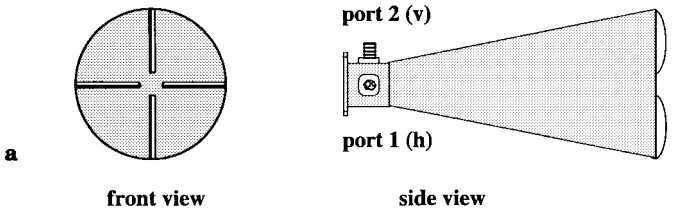

Fig. 13. Wide-band dual-polarized horn (2–18 Ghz) (horn 2).

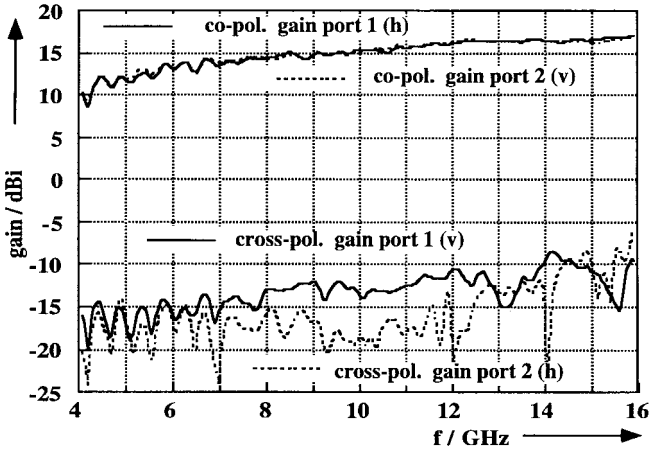

Fig. 15. Copolarized and cross-polarized gain G^t of the dual-polarized broad-band horn 2 (from Fig. 13) for ports 1 and 2, respectively.

network analyzer. Excellent agreement is achieved between both measurements, even down to values less than -20 dB. The discrepancy between RCS and VNwa measurement is partly due to the fact that the VNwa measurement was not carried out in an anechoic chamber, but in a laboratory room, which caused room reflections. Recently, an interesting intercomparison of horn gain was published by Stubenrauch [17]. The horn measured in this intercomparison differs from the one in Fig. 7. As a comparison with the measurements of [17] is not readily available, a comparison of the RCS method and a standard two-antenna method is shown in Fig. 17. For the measurement, both antennas were assumed to be identical. No near-field correction was applied. It shows that the "errors" are of the same order as in [17].

B. Dual-Polarized Broad-Band Horn Antenna

A typical antenna with two excitation ports is shown in Fig. 13. This wide-band horn has two separate feed ports for two orthogonal linear polarizations. This antenna is analyzed (Figs. 14–16) to verify the two-port equations. In Fig. 14, the resulting antenna polarization is depicted. The measured ellipticity angle is within $\pm 2°$ for both antenna subsystems over the entire frequency range from 4 to 16 GHz, which means that the horn is linearly polarized. When feeding port 1, the orientation angle is $\psi = 0°$, indicating that the copolarization is horizontal; for feeding at port 2 the orientation angle is $\psi = 90°$ and, thus, the radiated wave is vertically polarized.

Fig. 15 shows the copolarized and cross-polarized gain G^t for the two subsystems of the wide-band horn antenna. As the copolarization is horizontal for port 1, the corresponding cross-polar gain is vertical. For feeding at port 2, the copolarized gain is vertical and the cross-polarized gain is horizontal. The cross polarization is approximately 35 dB below the copolarization, but more than 20 dB above the system's polarization purity.

Some restrictions have to be made for the determination of the parameters $\underline{S}_{21}$ and $\underline{S}_{12}$ that describe the coupling between the two excitation ports of the antenna. It turns out that a direct calculation of the product term $\underline{S}_{12}\underline{S}_{21}$ from (8) fails both by direct matrix inversion and by using a Gaussian equation solver. The reason is that the S-parameter coefficients included in (8), which describe the cross-polar transfer characteristics, are very small. This leads to numerical instabilities. However, by assuming antenna reciprocity ($\underline{S}_{ih} = \underline{S}_{hi}$, $\underline{S}_{iv} = \underline{S}_{vi}$, $\underline{S}_{12} = \underline{S}_{21}$) (8) can be considerably simplified and the $\underline{S}_{21}\underline{S}_{12}$ product term can be extracted from a product that is mainly influenced by high-level copolarized transfer coefficients. The average values of the resulting coupling coefficients $\underline{S}_{21} = \underline{S}_{12}$ correspond very well to the direct VNwa measurement as depicted in Fig. 16. The ripple in the VNwa measurement may result from a long-line effect.

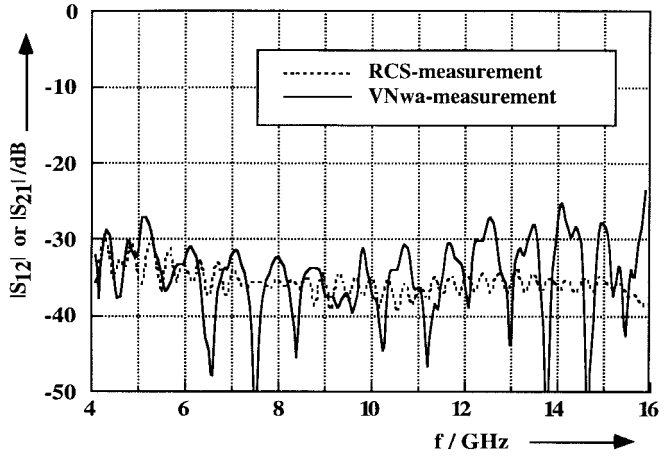

Fig. 16. Feed-line coupling between ports 1 and 2 of the dual-polarized broad-band horn 2 (from Fig. 13).

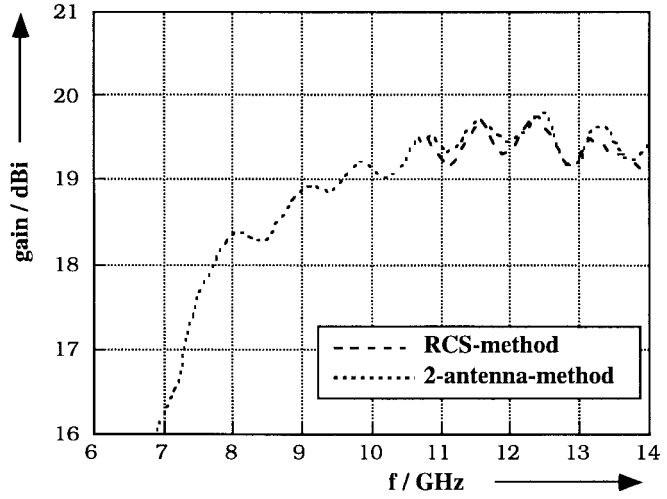

Fig. 17. Comparison of the gain measured by the RCS method and the two-antenna method for horn 1 (Fig. 7).

This is a quite impressive result considering that the decoupling between the antenna feeds is of the order of 35 dB and that this result can be determined from the free-space RCS antenna measurement procedure.

VI. Considerations and Conclusion

All measurement procedures have limitations—also the presented one. The accuracy of the RCS antenna measurement procedure is mainly determined by the accuracy of the RCS measurement. Calibration and polarimetric error correction enable RCS accuracies of better than 0.3 dB in magnitude and 3° in phase over a wide dynamic range. The calibrated polarization purity is better than 55 dB. Nevertheless, the measurement procedure is limited by some other factors. Since the AUT should be illuminated with a plane wave, far-field requirements have to be fulfilled. This limits the size and/or measurement distance. Short distances allow only small antennas at a given frequency. For long ranges, the measurement dynamic range might be a problem. Since a quasi-monostatic setup is used, a residual angle remains between transmit antenna, the AUT, and the receive antenna. For antennas with narrow beams, this will cause errors in the measured gain since incident and reflected waves do not enter the AUT in boresight direction. However, this problem can be overcome by a truly monostatic measurement system.

Despite these considerations, the presented measurement technique gives the most complete and accurate information about antenna radiation, antenna characteristics, and scattering obtainable with one single measurement setup only. Some quantities determined here, such as the maximum available gain and the polarization characteristics, are difficult to access with standard antenna transmission measurements, as with the two- or the three-antenna methods [10], [17]. The procedure can handle extremely wide bandwidths, i.e., 2–40 GHz, with an absolute gain calibration like no other measurement setup. No reference cable from the antenna to the receiver is necessary. This helps to avoid some difficulties usually experienced with other measurement procedures.

References

[1] D. D. King, "Measurement and interpretation of antenna scattering," *Proc. IRE*, vol. 37, pp. 770–777, July 1949.
[2] R. J. Garbacz, "Determination of antenna parameters by scattering cross-section measurements," *Proc. Inst. Elect. Eng.*, vol. 111, no. 10, pp. 1679–1686, Oct. 1964.
[3] J. Appel-Hansen, "Accurate determination of gain and radiation patterns by radar cross-section measurements," *IEEE Trans. Antennas Propagat.*, vol. AP-27, pp. 640–646, Sept. 1979.
[4] J. J. H. Wang, C. W. Choi, and R. L. Moore, "Precision experimental characterization of the scattering and radiation properties of antennas," *IEEE Trans. Antennas Propagat.*, vol. AP-30, pp. 108–112, Jan. 1982.
[5] D. M. Kerns, "Plane-wave scattering-matrix theory of antennas and antenna-antenna interactions: Formulation and applications," J. Res. Nat. Bur. Stand. (U.S.), vol. 80B, no. 1, pp. 5–51, Jan./Mar. 1976.
[6] K. M. Lambert, R. C. Rudduck, and T. H. Lee, "A new method for obtaining antenna gain from backscatter measurements," *IEEE Trans. Antennas Propagat.*, vol. 38, pp. 896–902, June 1990.
[7] E. Heidrich and W. Wiesbeck, "Features of advanced polarimetric RCS-antenna measurements," in *Conf. Proc. IEEE AP-S Int. Symp. URSI Radio Sci. Meet.*, San Jose, CA, June 1989, vol. II, pp. 1026–1029.
[8] ——, "Wideband polarimetric determination of antenna radiation and scattering characteristics by RCS measurements," in *Conf. Proc. 12th Antenna Measurement Tech. Assoc. Meet. Symp.*, Philadelphia, PA, Oct. 1990, pp. 10-33–10-38.
[9] ——, "Theoretical and experimental determination of the polarimetric antenna radar cross section," *Electromagn.*, vol. 14, pp. 99–117, 1994.
[10] H. Mott, *Antennas for Radar and Communication*. New York: Wiley, 1992.
[11] W. Wiesbeck and D. Kähny, "Single reference, three target calibration and error correction for monostatic, polarimetric free space measurements," *Proc. IEEE*, vol. 79, pp. 1551–1558, Oct. 1991.
[12] W.-M. Boerner, H. Mott, E. Lueneburg, W.-N. Boerner, H. Mott, E. Luenburg, B. Brisco, R. Brown, and J. S. Paterson, "Polarimetry in remote sensing: Basic and applied concepts," *The Manual of REMOTE SENSING*, 3rd ed., R. A. Reyerson, Ed. Bethesda, MD: Amer. Soc. Photogrammetry Remote Sensing (ASPRS) Publ., 1997, ch. 5.
[13] V. H. Rumsey, G. A. Deschamps, M. L. Kales, and J. I. Bohnert, "Techniques for handling elliptically polarized waves with special reference to antennas—Part II," *Proc. IRE*, vol. 39, pp. 540–544, May 1951.
[14] IEEE Stand. Def. Terms Antennas, IEEE Std. 145-1983, New York, 1983.
[15] A. C. Newell and D. M. Kerns, "Determination of both polarization and power gain of antennas by a generalized three-antenna measurement method," *Electron. Lett.*, vol. 7, no. 3, pp. 68–70, Feb. 1971.
[16] E. Heidrich, "Theoretische und experimentelle Charakterisierung der polarimetrischen Strahlungs- und Streueigenschaften von Antennen," Ph.D. dissertation, Univ. Karlsruhe, Karlsruhe, Germany, May 1992 (in German).

[17] C. F. Stubenrauch, A. C. Newell, A. G. Repjar, K. MacReynolds, D. T. Tamura, F. H. Larsen, J. Lemenczyk, R. Behe, G. Portier, J. C. Zehren, H. Hollimann, J. D. Hunter, D. G. Gentle, and J. P. M. de Vreede, "International intercomparison of horn gain at X-band," *IEEE Trans. Antennas Propagat.*, vol. 44, pp. 1367–1374, Oct. 1996.

Werner Wiesbeck (SM'87–F'94) received the Dipl.Ing. (M.S.E.E.) and the Dr.Ing. (Ph.D.E.E.) degrees from the Technical University, Munich, Germany, in 1969 and 1972, respectively.

From 1972 to 1983, he was with AEG-Telefunken in various positions including that of Head of Research and Development of the Microwave Division, Flensburg, Germany, and Marketing Director of the Receiver and Direction Finder Division, Ulm, Germany. During this period he had product responsibility for millimeter-wave radars, receivers, direction finders, and electronic warfare systems. Since 1983 he has been Director of the Institut für Höchstfrequenztechnik und Elektronik (IHE) at the University of Karlsruhe, Germany, where he is presently Dean of the Faculty of Electrical Engineering. In 1989 and 1994, respectively, he spent a six-month sabbatical at the Jet Propulsion Laboratory, Pasadena, CA. He serves as a permanent Lecturer for radar system engineering and wave propagation for the Carl Cranz Series for Scientific Education. His research interests include radar, remote sensing, wave propagation, and antennas.

Dr. Wiesbeck is a member of the IEEE Geoscience and Remote Sensing (GRS) AdCom (1992–2000), Chairman of the GRS-S Awards Committee, GRS-S Executive Vice President (1998–1999), and Past Treasurer of the IEEE German Section. He has been General Chairman of the 1993 Conference on Microwaves and Optics (MIOP'93) and he has been a member of scientific committees of many conferences. He is a member of an Advisory Committee of the EU—Joint Research Center (Ispra/Italy) and he is an advisor to the German Research Council (DFG) and to the Federal German Ministries for Research and Telecommunication.

Eberhardt Heidrich (SM'88) was born in Kraichtal/Gochsheim, Germany in 1961. He received the Dipl.Ing. (M.E.E.) and the Dr.Ing. (Ph.D.E.E.) degrees from the University Karlsruhe, Germany, in 1987 and 1992, respectively.

From 1987 to 1993, he was with the Institut für Höchstfrequenztechnik und Elektronik (IHE), University Karlsruhe, as a Research Assistant, responsible for lectures in microwaves and antennas where he was also Head of the Antenna Laboratory. His research responsibilities during this period included RCS and antenna measurement, polarimetric calibration techniques, microstrip antennas, and radar system engineering. Since January 1994, he has been with L&S GmbH in Lichtenau (B-W), Germany, engaged in VHF/UHF wave propagation, microwave sytem engineering, and antenna design. He serves as a Lecturer for radar techniques for the Carl Cranz Series for Scienfific Education.

Dr. Heidrich is member of IEEE Microwave Theory and Techniques/Antennas and Propagation Societies and Antenna Measurement Techniques Association (AMTA). He was awarded an IEE International Conference on Antennas and Propagation Best Paper Award in 1991.